A&A manuscript no.
(will be inserted by hand later)

Your thesaurus codes are:
03 (04.19.1; 11.05.2; 11.16.1; 11.19.7; 12.12.1; 13.09.1)

ASTRONOMY AND ASTROPHYSICS

A wide field survey at the Northern Ecliptic Pole I: Number counts and angular correlation functions in K ⋆

M.W. Kümmel[1,2] and S.J. Wagner[1,⋆⋆]

[1] Landessternwarte Heidelberg-Königstuhl, Königstuhl 12, D-69117 Heidelberg, Germany
[2] (present address:) Max-Planck-Institut für Astronomie, Königstuhl 17, D-69117 Heidelberg, Germany

Received 5 May 1999/ Accepted November 5

Abstract. We present the results from a multi colour survey performed at the Northern Ecliptic Pole (NEP). The survey is designed to identify the counterparts of faint sources from the ROSAT All Sky Survey and the IRAS survey and to study their optical/near-infrared properties. We observed the central square degree around the NEP in the optical bands B_J and R and in the near-infrared band K. A shallower survey was carried out in the optical I band. Here we present the results of the K-band survey. We discuss the source counts in the magnitude range $7\,\mathrm{mag} < K < 17.5\,\mathrm{mag}$ and the angular correlation function of galaxies with $K < 17.0\,\mathrm{mag}$. The galaxy counts at the NEP display a subeuklidean slope in $\mathrm{d}\log N/\mathrm{d}m$. Our shallower slope does not require the large effects of galaxy evolution or density evolution suggested to explain the steeper slopes found in earlier surveys. The angular correlation function of galaxies follows a power law $w^t(\theta) = A\theta^{-\delta}$ with $A = (5.7\pm0.8)\times10^{-3}$ and $\delta = 0.98 \pm 0.15$. This is in accordance with the expected values for stable clustering.

Key words: Surveys – Galaxies: evolution – Galaxies: photometry – Galaxies: statistics – Cosmology: large-scale structure of Universe – Infrared: galaxies

1. Introduction

Since surveys by satellites obtained deep exposures at the Ecliptic Poles, the Northern Ecliptic Pole (NEP) is a special location in the sky. The total exposure time at the NEP in the ROSAT All-Sky Survey, for example, was $\leq 40\,000$ sec as compared to ≤ 400 sec at the ecliptic equator (Brinkmann et al. 1999). Likewise, the deepest part of the IRAS survey in the far infrared ($12 - 100\,\mu$m) is located at the NEP, reaching flux limits down to 60 mJy at $60\,\mu$m (Hacking & Houck 1987).

We took surveys in the optical/near-infrared regime to identify those sources and to study their broad band energy distribution. Our surveys cover the central square degree around the NEP and were carried out in the optical B_j- and R-band and in the near-infrared filter K. The 95% completeness limits in B_j, R, and K are 24.0 mag, 23.0 mag, and 17.5 mag, respectively. The results of the identification and details on our optical surveys will be given in separate papers. Here we give the number counts of galaxies and point like sources and present the galaxy two-point correlation function of our K-band survey, which is unprecedented as a homogeneous survey in dynamic range and angular size at this depth.

Galaxy number counts and galaxy correlation function are basic quantities in the investigation of galaxy evolution and galaxy distribution and have both been studied extensively in the optical regime. K-band selected samples have the advantage that the K-corrections are small and nearly independent of galaxy type (Poggianti 1997). Moreover the absolute magnitudes of galaxies in K are dominated by stars of $M \sim 1\,M_\odot$, which makes the near-infrared as a better tracer of the visible mass of galaxies as compared to the optical, where the absolute magnitudes may be strongly affected by star formation.

With the completeness limit of $K = 17.5$ mag our survey enters a very interesting magnitude range with a high statistical level given by the large field. In this magnitude range a break in the slope of the galaxy number counts from 0.67 to 0.26 has been claimed by combining shallow, large scale surveys with deeper surveys on small fields (Gardner et al. 1993). From our homogeneous wide, medium-deep survey we can determine the exact location of this break.

Our survey also bridges the gap between correlation functions measured in deep samples ($K \geq 18.5$ mag) which find amplitudes above the values expected for a non-evolving two-point correlation function (Roche et al. 1998, 1999) and those values from shallower samples ($K \leq 16.0$ mag, Baugh et al. 1996) which are in accor-

Send offprint requests to: M.W. Kümmel

⋆ Based on observations collected at the German-Spanish Astronomical Centre, Calar Alto, operated by the Max-Planck-Institut für Astronomie, Heidelberg, jointly with the Spanish National Commission for Astronomy

⋆⋆ Email:swagner@lsw.uni-heidelberg.de
Correspondence to: Kuemmel@mpia-hd.mpg.de

Table 1. The coordinates of the NEP field centre

α_{2000}:	18h 00m 00.0s	δ_{2000}:	$66^\circ\,33'\,38.6''$
l_{II}:	$96^\circ.38$	b_{II}:	$29^\circ.81$

dance with stable clustering (no evolution).

Table 2. Completeness and classification parameters

Bin	Area [deg^2]	$N_{\rm tot}$	$N_{\rm stat}$
$K < 16.0$ mag	0.93 deg^2	3572	4
16.0 mag $< K <$ 16.5 mag	0.93 deg^2	1430	10
16.5 mag $< K <$ 17.0 mag	0.91 deg^2	2080	120
17.0 mag $< K <$ 17.5 mag	0.61 deg^2	1733	371

2. Observation and data analysis

2.1. Observation and photometric calibration

The observations were made with the 2.2-m telescope on Calar Alto, Spain, during two observing runs from July 22 to 26, 1994 and August 8 to 10, 1995 using the NIR camera MAGIC (Herbst et al. 1993). This camera is equipped with a NICMOS 3 array, similar to the system described by Hodapp et al. (1992) with 256×256 HgCdTe diodes. In the *Wide Field Mode*, chosen for our project, the field size is $6.9' \times 6.9'$ with a scale of $1.6''$/pixel.
The coordinates of the NEP in various coordinate systems are given in Table 1. To cover the central square degree around the NEP, we observed a regular grid of 9×9 fields. On each field several images were taken on 16 different positions with non-integer pixel offsets in right ascension and declination between the individual positions. This dithering allows for averaging potential variations of the response on a sub-pixel scale as well as for corrections of individual hot pixels, both being essential in undersampled imaging. In a photometric night we carried out a snapshot survey where every field was observed in two positions to obtain homogeneous photometry. Including the snapshot survey the total integration time per field is 648 sec. The data were obtained using a K'-filter (Wainscoat & Cowie 1992) with central wavelength $\lambda_{central} = 2.10\,\mu$m and $\Delta\lambda = 0.34\,\mu$m width (Herbst 1995).
In a photometric night we observed NIR standard stars from the lists of Elias et al. (1982), Zuckermann & Becklin (1987), and Casali & Hawarden (1992) and used the K-magnitudes to determine zero point and extinction. Within the range $-0.036\,\text{mag} \le H - K \le 0.325\,\text{mag}$ covered by the standard stars, the zero point does not depend on colour in $H - K$.
Flux calibration was established using the snapshot survey taken within three consecutive hours in a single photometric night. These data were reduced and coadded independently from the main survey to obtain a homogeneous set of photometric zero-points. This was transferred to the deeper, coadded survey data for each field individually, using several stars in every case.

2.2. Standard reduction

Standard reduction included dark subtraction, sky subtraction, and flatfield division of the individual images. Dark exposures were taken during daytime with the same camera settings that were used for the scientific exposures, and flatfields were constructed from the differences between images of an illuminated and dark screen in the dome. For every field a sky frame was constructed by scaling the dark corrected exposures of this field to the same level multiplicatively and removing the objects by computing the median for each pixel.
The spatial offsets of the images taken on different positions within one field were determined using bright stars. Before coadding the images were resampled to a grid with $0.4''$ pixels. Due to the resampling it was possible to coadd the images on a finer grid. This resulted in a better definition of the objects shape and a stable performance of the source-detection routines.
Further analysis was then done only on the central area of each field which was observed with the full integration time. This leaves an effective survey area of 0.93 deg^2, spread over the full square degree with small gaps between adjacent fields.

2.3. Object detection and photometry

The detection of sources was carried out with FOCAS (Valdes 1994, Jarvis & Tyson 1981). We tested the reliability of the detection process as a function of the input parameters on three fields which were observed with an integration time of 2 160 sec, more than three times the amount spent on the other survey fields. In these fields we coadded the total of all images to deep frames as well as subsets of images to frames of integration times and depths equal to those of the entire survey. Then we performed source detection on all frames with various sets of detection parameters. The reliability of the detection was analyzed by identifying the objects detected on the shallower frames in the deeper ones. The detection parameters for the survey were chosen such that only $< 1\,\%$ of the sources in the shallow frames could *not* be found in the deep frames, which gives a reliability of $> 99\,\%$ for the sample of the detected objects. This high reliability was achieved by accepting objects above 16 σ only.
FOCAS performs different types of photometry: the isophotal flux L_i is measured within the detection area, the so called total flux L_{total}, which is determined in the area expanded by a factor two around the detection area and the flux measured within a specified aperture around the object, L_{lfca}. L_{total} has the advantage to give good flux estimates independent from the extent of the objects,

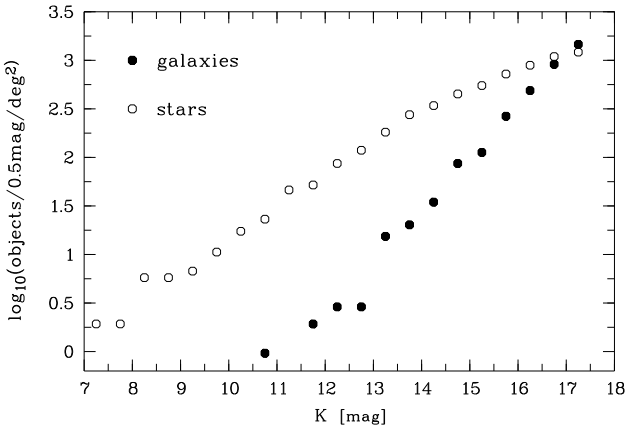

Fig. 1. The number density for extended and point-like sources, labeled as galaxies and stars, respectively.

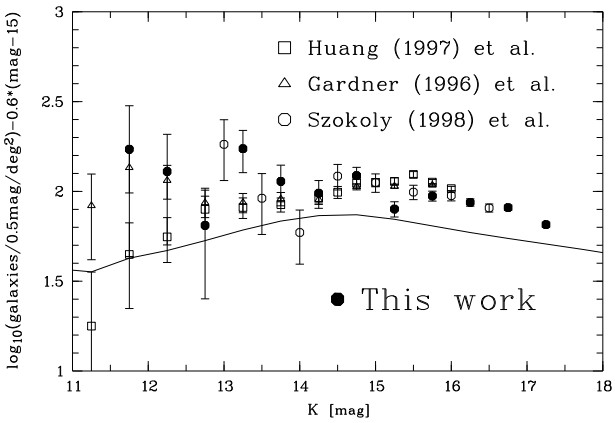

Fig. 2. The galaxy counts from the NEP compared to the results of other surveys covering areas on the square degree scale. The solid line shows predicted counts from Jimenez & Kashlinsky (1999) (their $\Omega_0 = 0.2$, $\Omega_\Lambda = 0.0$ model).

because the flux is determined in an area adapted to object sizes. However, L_{total} misses flux at the faint level (see e.g. Saracco et al. 1997). To take this into account we chose L_{total} for the bright sources and L_{lfca}, measured in an aperture of 7.2″ diameter, for the faint sources. The final value depends on the size of the object. If L_{total} is determined in an area *smaller than* 41 arcsec^2 (the area corresponding to the diameter of the aperture), L_{lfca} is used instead. The transition from L_{total} to L_{lfca} occurs at $K \sim 16.5$ mag. We compared the magnitudes of the same objects found on the set of shallow and deep frames mentioned above to confirm that the magnitude differences are caused by statistically distributed measurement errors and did not detect any systematic trend.

2.4. Morphological classification

Since the point spread function (PSF) of the K-images is grossly undersampled, we made no attempt to classify the objects on the basis of the K-data. Instead, the objects were classified on the basis of the morphological identifying of their counterparts in the R-survey which has an effective PSF of $\sim 1.2''$. In the R-survey (of which details are given in Kümmel 1998 and Kümmel & Wagner in prep.) the classification is based on the *FOCAS resolution classifier* (Valdes 1982). The classification into point-like and extended objects is reliable for objects $R \leq 21.5$ mag. Towards fainter magnitudes extended objects are progressively misclassified as point-like objects because their extended parts vanish in the background noise. In the R band we use a statistical classification by extrapolating the number-counts of point-like objects ($\mathrm{d}\log N/\mathrm{d}m = const$) into the range of unreliable classification to estimate the fraction of extended objects. The (small) fraction of sources detected in K whose R-band counterparts are too faint for a reliable morphological classification were divided into point-like and extended sources based on the fraction of these types at the corresponding magnitudes of the R-band counterparts. This is strictly valid only if point-like and extended objects have similar R-K colour for $R \leq 21.5$ mag

2.5. Completeness

The completeness was determined using the set of deeper images with longer integration times, mentioned in Sect. 2.3 which were used already to find the optimum set of detection parameters. The object lists of those images were divided into those found in the shallower images and those found only in the deep images. This ratio was fitted by a completeness function $f(mag)$

$$f(mag) = \left[\exp\left(\frac{mag - mag_{50}}{b}\right) + 1\right]^{-1} \quad (1)$$

with mag_{50} being the magnitude where 50 % of the objects detected in the deeper images have been found in the shallower images. The parameter b is a measure of the width $\Delta mag = mag_2 - mag_1$ where completion drops from $f(mag_1) = 1-\epsilon$ to $f(mag_2) = \epsilon$. We fitted $f(mag)$ to a series of deep/shallow matches taken under different conditions with different image quality. While b was found to be independent of image quality ($b = 0.26$), mag_{50} varies by 0.3 mag, reflecting the basic parameters of image quality, i.e. background noise and FWHM of the PSF. Establishing the relations between those parameters and mag_{50} and using these relations and the corresponding zero points we computed mag_{50} for every individual survey image. We finally set a completeness limit $mag_{compl} = mag_{50} - 0.5$. Down to this level $f(mag)$ was found to be > 0.9 (i.e. indistinguishable from 1.0) in our deep fields. We do not use $f(mag)$ to correct counts fainter than mag_{compl} in this study.

Table 3. Quantitative comparison of galaxy counts

Survey	area	slope	amplitude	range
NEP_a	0.93	0.56 ± 0.01	97 ± 4	10.5-17.0
NEP_b	0.93	0.41	175	16.5-17.5
Szokoly	0.6	0.56 ± 0.02	98 ± 5	12.75-16.75
Huang	9.8	0.65 ± 0.01	103 ± 2	11.0-16.0
Gardner	9.8	0.63 ± 0.01	103 ± 2	10.0-16.0

3. Source counts

3.1. Star and galaxy counts

Fig. 1 displays the object counts for point-like and extended source, labeled as stars and galaxies, respectively. No attempt was made to correct object counts beyond mag_{compl} as defined in Sect. 2.5. The counts were derived only from fields complete to the specific magnitude. The area of the sub-surveys complete to various depths are given in Table 2. Furthermore, Table 2 shows the number of objects with statistical classification in R, $N_{\rm stat}$, and the total object number in that bin, $N_{\rm tot}$.

The star counts are in good agreement with the theoretical expected values from Wainscoat et al. (1992), calculated for $l_{II} = 90°.0$, $b_{II} = 30°.0$, which is in the vicinity of the NEP (see Table 1).

For $K < 17.0$ mag the galaxy counts are well approximated by a power law with $\mathrm{d}\log N/\mathrm{d}m = 0.56$. The counts in the faintest bin differ significantly from this slope and the two faintest bins result in $\mathrm{d}\log N/\mathrm{d}m = 0.41$, establishing a break or the beginning of a roll-over in the range $16.5 < K < 17.0$. Both the bright and the faint end slope are *below* the Euclidean value of $\mathrm{d}\log N/\mathrm{d}m = 0.6$.

3.2. Interpretation of the galaxy number counts

To compare our galaxy counts with the numbers from other surveys covering areas $> 0.6\,\mathrm{deg}^2$, Fig. 2 gives our data together with the counts from Gardner et al. (1996), Huang et al. (1997) and Szokoly et al. (1998). In Fig. 2 the Euclidean slope 0.6 has been subtracted from the logarithm of the counts in order to expand the ordinate and to make differences between the counts clearly visible.

We fitted power laws of the form

$$N(mag) = a * 10^{b*(mag-15.0)} \qquad (2)$$

to the counts plotted in Fig. 2 and give the parameters of those fits as well as quality estimators in Table 3. The first two columns give the reference and the survey area (in deg^2). Then the slope b, the amplitude a, and magnitude range of the fits are listed. The counts at the NEP are split into two regimes, referenced as NEP_a and NEP_b, because counts at the faint end (NEP_b) do not follow the extrapolation of the power-law of the $K \leq 17.0$ mag objects (NEP_a in Table 3).

The normalization of the power-laws for the different galaxy counts with $K \leq 16.5$ mag, listed in Table 3, agree well among each other within the errors. The slopes of the power laws differ. While the surveys of Gardner et al. (1996) and Huang et al. (1997) find values around $b \approx 0.64$, the galaxy counts of Szokoly et al. (1998) and at the NEP both result in the subeuklidean value $b = 0.56$. The difference between those two groups can be seen clearly at the counts in Fig. 2. Power-law fits to the data points from Gardner et al. (1996) or Huang et al. (1997) have a positive slope, which means a supereuklidean slope for the pure counts, whereas fits to the data from Szokoly et al. (1998) and the NEP have negative slopes corresponding to a subeuklidean slope for the pure counts in $\mathrm{d}\log N/\mathrm{d}m$.

Huang et al. (1997) explain the large slope of their counts with a local under-density of galaxies. Quantitatively they determine that the normalization of the luminosity function doubles its value from $z = 0$ to 0.2. Phillips & Turner (1998) analyze all K-band counts to $K = 17.0$ mag known to mid-1997 and find two possible explanations for the steep slope: Either an evolution of the normalization of the galaxy luminosity function by a factor $1.7 - 2.4$ to a redshift of $0.1 - 0.23$ or an unexpectedly strong low redshift evolution in K which leads to evolutionary and cosmological corrections as much as 60 % larger than accepted values.

Our shallow, subeuklidean slope of the galaxy counts at the NEP argues against a local underdensity of galaxies or strong luminosity evolution. The value $\mathrm{d}\log N/\mathrm{d}m = 0.56$ is even smaller than the range $0.602 - 0.623$, which were computed in Huang et al. (1997) for different luminosity functions and cosmological corrections based on *constant* galaxy luminosities.

Gardner et al. (1993) reported a break in the slope of the galaxy number counts from $\mathrm{d}\log N/\mathrm{d}m = 0.67$ to 0.26. That break was claimed to occur between $K \approx 15.0$ mag and $K \approx 18.0$ mag. Our data at the NEP show with high statistical significance that this break in slope is less extreme, and starts at $K \approx 16.5$ mag with a flattening to 0.41 at $K \approx 17.5$ mag. A further flattening to slopes < 0.3 must occur at magnitudes $K > 17.5 - 18.5$ mag to match number densities to deeper source counts from e.g. Moustakas et al. (1997) and Djorgovski et al. (1995).

Subeuklidean counts in the magnitude range $K = 15.0 - 17.0$ mag are supported by the recent compilation of galaxy evolution models from Jimenez & Kashlinsky (1999). In their model the density of galaxies is assumed to be independent of redshift. Their predicted K-band counts (for $\Omega_0 = 0.2$ and $\Omega_\Lambda = 0.0$) are shown with the solid line in Fig. 2. Although there is an offset in the normalization of ~ 0.15 dex with respect to *all* data displayed in Fig. 2, the slope of the predicted counts drops below euklidean values at $K \geq 14.8$ mag.

4. Angular correlation function

Table 4. The angular correlation function for the various samples

Sample selection		Number of	A free, δ fixed			A and δ free		
K [mag]	R-K [mag]	galaxies	A [10^{-3}]	δ	σ^2/A	A [10^{-3}]	δ	σ^2/A
12.0 - 16.0	all	491	9.97 ± 2.77	0.8	1.83	2.78 ± 3.42	1.14 ± 0.27	2.84
16.0 - 17.0	all	1234	5.75 ± 1.07	0.8	1.84	2.33 ± 2.13	1.02 ± 0.21	2.44
12.0 - 17.0	all	1725	5.70 ± 0.77	0.8	1.83	2.77 ± 1.78	0.98 ± 0.15	2.30
12.0 - 17.0	>3.49	858	9.23 ± 1.55	0.8	1.85	3.12 ± 2.47	1.08 ± 0.18	2.81
12.0 - 17.0	<3.49	867	7.30 ± 1.52	0.8	1.83	3.48 ± 3.50	0.99 ± 0.23	2.32

4.1. The calculation of the angular correlation function

The angular correlation function $w(\theta)$ is defined by

$$\mathrm{d}P = N^2[1 + w(\theta)]\,\mathrm{d}\Omega_1\,\mathrm{d}\Omega_2, \tag{3}$$

where N is the mean density of galaxies per steradian and $\mathrm{d}P$ the joint probability of finding one galaxy within the solid angle $\mathrm{d}\Omega_2$ in the projected distance θ away from a galaxy within the solid angle $\mathrm{d}\Omega_1$ (Groth & Peebles 1977). $w(\theta)$ is determined by assembling the normalized histograms of logarithmic distances for the data sample, $\langle DD\rangle$, a random sample, $\langle RR\rangle$, and for the data-random sample, $\langle DR\rangle$, and applying (Landy & Szalay 1993):

$$w(\theta) = \frac{\langle DD\rangle - 2\langle DR\rangle + \langle RR\rangle}{\langle RR\rangle} \tag{4}$$

The measured function $w^m(\theta)$ computed in Eq. (3) is biased towards low values with respect to the true function, $w^t(\theta)$, by

$$w^m(\theta) = w^t(\theta) - \sigma^2 \tag{5}$$

(Baugh et al. 1996, Roche & Eales 1998, Lidman & Peterson 1996), but this bias σ^2 can be estimated as

$$\sigma^2 \approx \frac{1}{\Omega^2}\int w^t(\theta_{12}) d\Omega_1\, d\Omega_2 \tag{6}$$

(Groth & Peebles 1977). The angular correlation function is usually described by a power-law $w^t(\theta) = A\theta^{-\delta}$. If the exponent δ is known, the amplitude of $w^t(\theta)$ is determined by fitting the measured correlation to the function

$$w^m(\theta) = A(\theta^{-\delta} - \sigma^2/A). \tag{7}$$

If the value for δ is not known, Eq. (6) and Eq. (7) have to be iterated.

4.2. $w(\theta)$ of galaxies $K < 17$ mag

We calculated the angular correlation function of galaxies brighter than $K = 17$ mag. To avoid spurious detection of the filaments around the planetary nebulae NGC 6543 a sufficiently large region was masked out, leaving a sample of 1725 objects in an area of 0.9 deg^2. Following Baugh et al. (1996) we use

$$\delta w^m(\theta) = 2 * \sqrt{(1 + w^m(\theta))/[DD])} \tag{8}$$

to derive errors, were $[DD]$ denotes the *non* normalized histogram of $\langle DD\rangle$.

Table 4 give the results of fitting $w^m(\theta)$ to Eq. (7) in case for a fixed $\delta = 0.8$ and for δ being a free parameter. This was computed for the total sample as well as for subsamples split at $K = 16$ mag.

Fig. 3 shows the bias-corrected angular correlation function of the total sample with the power law fitted to the data ($\delta = 0.8$) on scales $10'' < \theta < 33'$. While the lower limit is dictated by the small number of pairs in $[DD]$, the upper limit is set to half the largest size of the survey field. The measured correlation follows the power law very well on all scales. There is no indication of a break or discontinuity on the scale of the distance between two adjacent fields (marked by the arrow in Fig. 3). Even the largest deviation at the widest angular scale ($\theta = 0.44°$) is at the level of 2.5 σ, i.e. not significant.

With a power-law slope of $\delta \sim 1.0$, and range of more than two orders of magnitude in θ, a strong variation of the surface density about the mean value of 0.5 arcmin^{-2} is implied. Due to the still low average surface density, the peaks in the surface density distribution cannot be attributed to clusters in an unambiguous way.

We investigated whether the angular correlation depends on galaxy colour. The total set of objects is divided into a red sample with $R - K > 3.49$ mag and a blue sample with $R - K < 3.49$ mag. The two subsamples are selected to include approximately the same number of objects (see Table 4). The angular correlation function was computed in the same way as for the total sample and values for the amplitude and scale-length derived from the fits to the correlation functions are given in Table 4.

Fig. 3 shows the bias corrected correlation functions of the blue and the red sample in comparison to the total sample. As can be seen in Fig. 3 and in Table 4 within the errors the blue galaxies show the same clustering properties as the red galaxies.

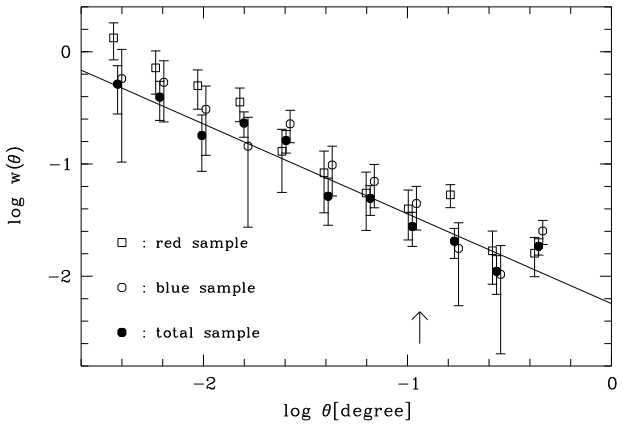

Fig. 3. $w^t(\theta)$ for the $K \leq 17.0$ mag and for blue and the red subsamples. Abscissa values of the red and the blue sample were offset by $\Delta \log(\theta) = \pm 0.02$. The solid line displays the power law fitted to the total sample ($\delta = 0.8$) and the arrow indicates the separation between two adjacent fields

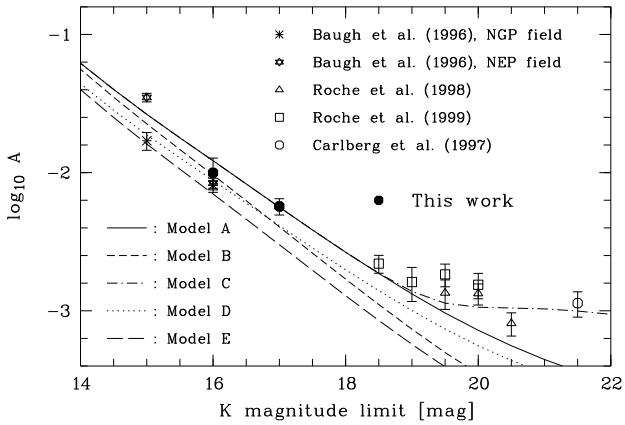

Fig. 4. The $w(\theta)$ amplitude of galaxies in our survey at the NEP, compared with amplitudes from the surveys of Baugh et al. (1996), Roche et al. (1998, 1999) and Carlberg et al. (1997). The lines show the theoretical models from Roche et al. (1998, 1999).

4.3. The angular correlation function of K-selected galaxies

The two-point correlation function is approximated by a power-law with two free variables. It is important to note that these are not derived independently. The comparison of the amplitude of the correlation is subject to differences in the angular range involved in the fitting even for fits with fixed slopes δ.

Fig. 4 gives the change of amplitudes of the angular correlation function with limiting magnitude in K. The values determined in Sect. 4 are displayed together with all other measurements known to us (from Baugh et al. 1996, Carlberg et al. 1997, Roche et al. 1998, 1999). From Baugh et al. (1996) two values for the amplitude are given in Fig. 4 since the amplitude obtained in two different fields are discrepant at the bright end.

The lines in Fig. 4 show the theoretically expected values for the amplitude of the angular correlation function as computed in Roche et al. (1998, 1999) for various models of the spatial two-point correlation function. Details of those models can be found in these papers and references therein.

The amplitude of our $K < 16.0$ mag galaxies is in accordance with the values from Baugh et al. (1996) and does not exclude any of the models A to E due to the large error. The amplitude at the faint level is in good agreement with the values expected from models A and C. The difference between the data and models B and D is $2.2\,\sigma$, thus these models cannot be rejected. Model E is rejected at the $3.3\,\sigma$ level. We want to point out that the amplitudes compared in Fig. 5 are derived assuming $\delta = 0.8$. Piecewise fits of $w^m(\theta)$, shown in Fig. 3 reveal that narrow angle surveys would obtain lower normalization and wide angle surveys larger ones. Comparison of $\mathrm{d}A/\mathrm{d}K$ as shown in Fig. 5 rely on $w^m(\theta)$ being well described by a single power-law.

Our data favour model A and C, which were computed assuming stable clustering and a significant higher normalization of the clustering strength for early type galaxies, as measured by Guzzo et al. (1997).

A stronger clustering of early type galaxies should result in a larger angular correlation amplitude for red galaxies. This is in contradiction to the results from Sect. 4.2 where the amplitude of the red sample (early type galaxies), was *not* significantly larger than the amplitude of the blue sample (late type galaxies). This disagreement could be caused by the diluting effects of the K-band selection of the sample which results in a broader distribution of the red galaxies in $\mathrm{d}N/\mathrm{d}z$ (Roche et al. 1999) and a decrease in the angular correlation amplitude of the red sample. This would still imply the existence of several nearby clusters with increased numbers of early-type galaxies, which are not detected.

Finally, we want to stress that further confirmation for the high correlations (see Fig. 4) found in $K > 19.0$ mag samples is needed despite existing measurements of the angular correlation function in samples down to $K = 21.5$ mag (Carlberg et al. 1997). Due to the small sample sizes used in these studies, the derivation of amplitudes (four times smaller than those found at K<17 in the present study) are dominated by Poisson errors and uncertainties introduced by the correction for stellar contamination. The measurement of the small signals expected at $K \sim 19$ mag would require samples of several 10^4 sources which are not yet available.

Acknowledgements. The authors want to thank N. Roche and R. Jimenez for providing us in digital form their model results

for the angular correlation function and galaxy number counts, respectively. This work was supported by the DFG (Sonderforschungsbereich 328) and the *Studienstiftung des deutschen Volkes*.

References

Baugh C. M., Gardner J. P., Frenk C. S., Sharples R. M., 1996, MNRAS 283, L15
Brinkmann W., Chester M., Kollgaard R., et al., 1999, A&AS, 134, 221
Carlberg R. G., Cowie L. L., Songaila A., Hu E. M., 1997, ApJ 484, 538
Djorgovski S., Soifer B. T., Pahre M. A., et al., 1995, ApJ 438, L13
Casali M., Hawarden T., 1992, UKIRT Newsletter 4, 33
Elias J. H., Frogel J. A., Matthews K., Neugebauer G., 1982, AJ 87, 1029
Gardner J. P., Cowie L. L., Wainscoat R. J., 1993, ApJ 415, L9
Gardner J. P., Sharples R. M., Carrasco B. E., Frenk C. S., 1996, MNRAS 282, L1
Groth E. J., Peebles P. J. E., 1977, ApJ 217, 38
Guzzo L., Strauss M. A., Fisher K. B., Giovanelli R., Haynes M., 1997, ApJ 489, 37
Hacking P., Houck J. R., 1987, ApJS 63, 311
Herbst T. M., 1995, Magic Observer's Guide, Max-Planck-Institut für Astronomie, Heidelberg
Herbst T. M., Beckwith S. V. W., Birk Ch., et al., 1993, in: Infrared Detectors and Instrumentation, ed. Fowler A. M., SPIE Proceedings Series, Vol. 1946, p. 605
Hodapp K. W., Rayner J., Irwin E., 1992, PASP 104, 441
Huang J. S., Cowie L. L., Gardner J. P., et al., 1997, ApJ 476, 12
Jarvis J. F., Tyson J. A., 1981, AJ 86, 476
Jimenez R., Kashlinsky A., 1999, ApJ 511, 16
Kümmel M. W., 1998, Ph. D. Thesis, University of Heidelberg
Landy S. D., Szalay A. S., 1993, ApJ 412, 64
Lidman C. E., Peterson B. A., 1996, MNRAS 279, 1357
Moustakas L. A., Davis M., Graham J. R., et al., 1997, ApJ 475, 445
Phillips L. A., Turner E. L., 1998, submitted to ApJ (astro-ph/9802352)
Poggianti B. M., 1997, A&AS 122, 399
Roche N., Eales S. A., 1999, MNRAS 307, 303
Roche N., Eales S. A., Hippelein H., 1998, MNRAS 295, 946
Roche N., Eales S. A., Hippelein H., Willott C. J.,1999, MNRAS 306, 538
Saracco P., Iovino A., Garilli B., Maccagni D., Chincarini G., 1997, AJ 114, 887
Szokoly G. P., Subbaro M. U., Connolly A. J., Mobasher B., 1998, ApJ 492, 452
Valdes F., 1982, in: Instrumentation in Astronomy IV, ed. Crawford D. L., S.P.I.E. Proceedings Series Vol. 331, p. 465
Valdes F., 1994, IRAF Group - Central Computer Services, National Optical Astronomy Observatories, Tucson
Wainscoat R. J., Cowie L. L., 1992, AJ 103, 332
Wainscoat R. J., Cohen M., Volk K., Walker H. J.,Schwartz D. E., 1992, ApJS 83, 111
Zuckerman B., Becklin E. E., 1987, ApJ 319, L99